Supporting Information

Hot-Injection Synthesis of $PtCu_3$ Concave Nanocubes with High-index Facets for Electrocatalytic Oxidation of Methanol and Formic Acid

Jiarun Geng, Zhuo Zhu, Xiaoxiao Bai, Fujun Li* and Jun Chen

Key Laboratory of Advanced Energy Materials Chemistry (Ministry of Education), Renewable Energy Conversion and Storage Center (RECAST), College of Chemistry, Nankai University, Tianjin 300071, China

*E-mail: fujunli@nankai.edu.cn

Chemicals and materials

Chloroplatinic (IV) acid hexahydrate ($H_2PtCl_6{\cdot}6H_2O$, 38%−40% Pt), copper (II) acetate dihydrate ($Cu(CH_3COO)_2{\cdot}2H_2O$, 99%), cetyltrimethylammonium bromide (CTAB, 99%), and trinoctylphospine oxide (TOPO, 99.9%) were purchased from J&K. Tetrabutylammonium bromide (TBAB, 99%), potassium bromide (KBr, 99%), and potassium chloride (KCl, 99%) were purchased from Tianjin Guangfu. Oleylamine (OAm, 80%−90%), oleic acid (OA, 99%), and carbon black (Vulcan XC−72) were purchased from Macklin. Absolute ethanol (99.9%), cyclohexane (99%), and *N*,*N*−Dimethylformamide (DMF, 99%) were provided by Tianjin Concord Co., Ltd. The commercial Pt/C (Pt/C, 20 wt% Pt) was purchased from Johnson Matthey. All chemicals and materials were used without further purification.

Calculations of Electrochemical Surface Area

The electrochemical surface areas ($ECSA_H$) were calculated by integrating the hydrogen desorption charge on the CV curves which were measured in the solution of Ar-saturated 0.5 M H_2SO_4 with the potential from −0.2 to 1.0 V (vs Ag/AgCl) at 10 mV s^{-1}. The detailed calculation procedure is shown as follow:

$$ECSA_H\ (\mathrm{m^2\ g^{-1}}) = \frac{\mathrm{S_{H_{adsorption}}}\ (\mathrm{A{\cdot}V})}{0.21\ (\mathrm{mC\ cm^{-2}}){\cdot}\mathrm{m_{Pt}}\ (\mathrm{mg}){\cdot}v\ (\mathrm{mV\ s^{-1}})} \times 10^5$$

$$\mathrm{S_{H_{adsorption}}} = \int_{-0.2}^{1.0} i\ \mathrm{d}E\ (\mathrm{A{\cdot}\ V})$$

0.21 mC cm^{-2} is assumed as the required charge which corresponding to the adsorbed monolayer of hydrogen per unit area on Pt surface. m_{Pt} (mg) is the mass of Pt on working electrode. v (mV s^{-1}) is scan rate.

Similarly, the $ECSA_{CO}$ were calculated by integrating the CO oxidation charge on the CV curves of CO oxidation which were tested in the solution of Ar-saturated 0.5 M H_2SO_4 with the potential from −0.2 to 1.0 V (vs Ag/AgCl) at 10 mV s^{-1}.

$$ECSA_{CO}\ (\mathrm{m^2\ g^{-1}}) = \frac{\mathrm{S}_{\mathrm{CO_{adsorption}}}\ (\mathrm{A{\cdot}V})}{0.42\ (\mathrm{mC\ cm^{-2}}){\cdot}\mathrm{m_{Pt}}\ (\mathrm{mg}){\cdot}v\ (\mathrm{mV\ s^{-1}})} \times 10^5$$

$$\mathrm{S}_{\mathrm{CO_{adsorption}}} = \int_{0.35}^{0.60} i\ \mathrm{d}E\ (\mathrm{A{\cdot}\ V})$$

0.42 mC cm^{-2} is assumed as the required charge which corresponding to the oxydic monolayer of CO per unit area on Pt surface.

Calculation of the Reaction Equilibrium Constant

$PtCl_6^{2-}$ (aq) + 6Br^- (aq) → $PtBr_6^{2-}$ (aq) + 6Cl^- (aq) K^θ

The following primary cell was designed to calculate the reaction equilibrium constant at 101.325 kPa, 298.15 K.

(-) Pt (s) | $PtBr_6^{2-}$ ($a$$PtBr_6^{2-}$) || $PtCl_6^{2-}$ ($a$$PtCl_6^{2-}$) | Pt (s) (+)

$PtCl_6^{2-}$ (aq) +4e^- → Pt (s) +6Cl^- (aq) $\varphi^\theta_{\mathrm{PtCl_6^{2-}/Pt}} = 0.73$ V

$PtBr_6^{2-}$ (aq) +4e^- → Pt (s) +6Br^- (aq) $\varphi^\theta_{\mathrm{PtBr_6^{2-}/Pt}} = 0.61$ V

$$\ln K^\theta = \ln\frac{[\mathrm{PtBr_6^{2-}}][\mathrm{Cl^-}]^6}{[\mathrm{PtCl_6^{2-}}][\mathrm{Br^-}]^6} = \frac{E^\theta}{\frac{RT}{4F}} = \frac{\varphi^\theta_{\mathrm{PtCl_6^{2-}/Pt}} - \varphi^\theta_{\mathrm{PtBr_6^{2-}/Pt}}}{\frac{RT}{4F}} \approx 20.24$$

R (molar gas constant) = 8.314 J mol^{-1} K

F (Faraday constant) = 96484 C mol^{-1}

$$K^{\theta} \approx 6.17 \times 10^{8} \gg 1$$

It can be deduced that the stability constant for $PtBr_6^{2-}$ is much larger than that of $PtCl_6^{2-}$.

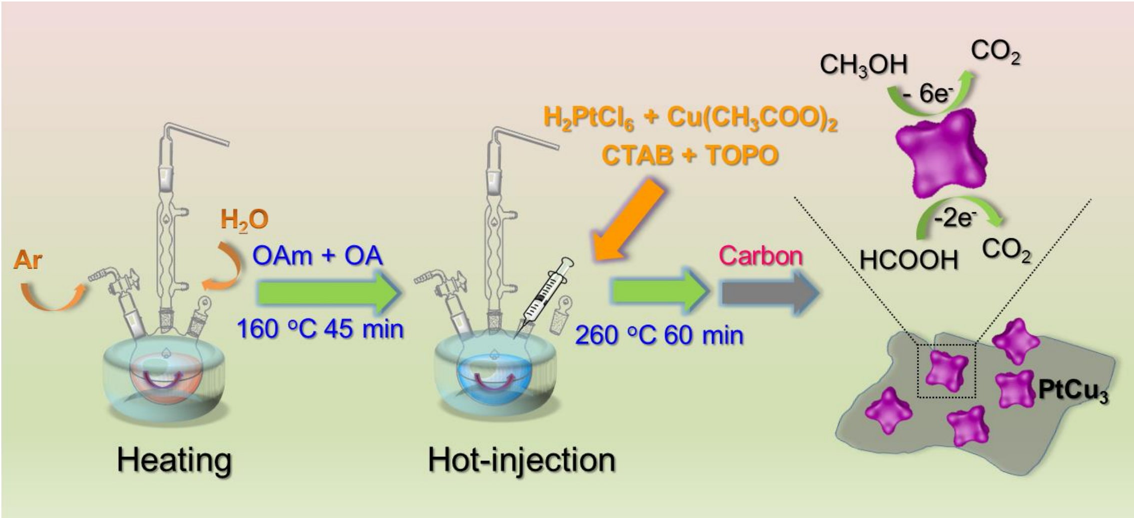

Figure S1. Schematic illustration of synthetic procedures of the $PtCu_3/C$ catalyst.

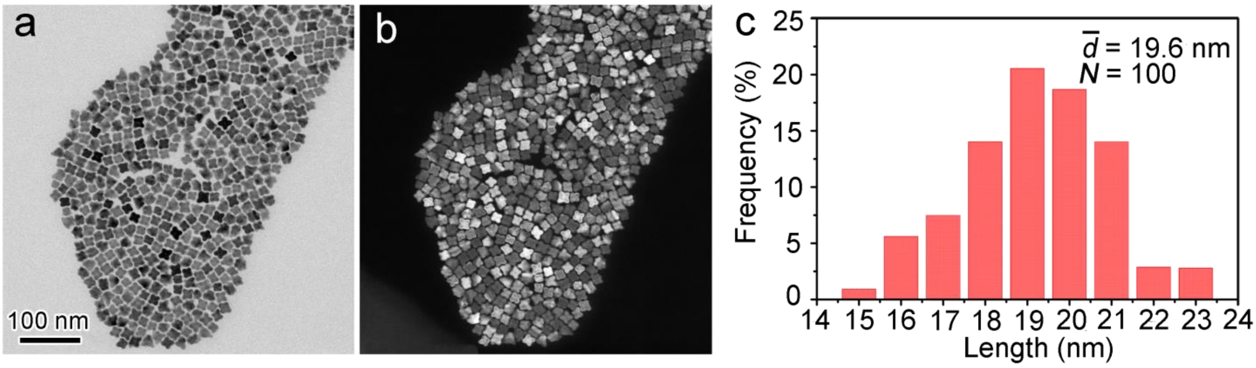

Figure S2. (a) Bright field, (b) dark field TEM images, and (c) particle size distribution of the $PtCu_3$ concave nanocubes.

Table S1. Atomic ratios of the $PtCu_3$ concave nanocubes determined by ICP-OES.

	1	2	3
Pt/Cu atomic ratio	1/2.92	1/2.92	1/3.05

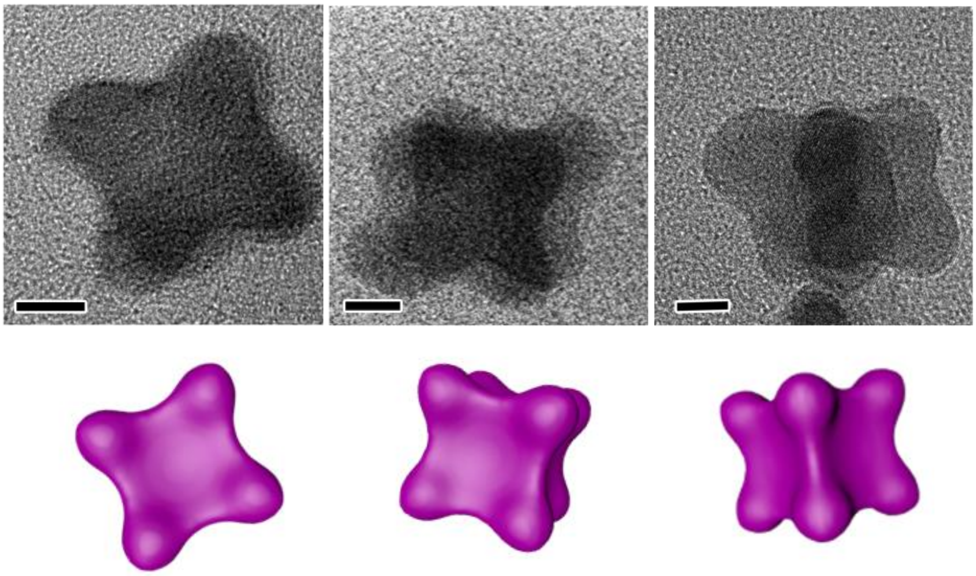

Figure S3. TEM images of the $PtCu_3$ concave nanocubes from different projections directions and their corresponding models with scale bars of 5 nm.

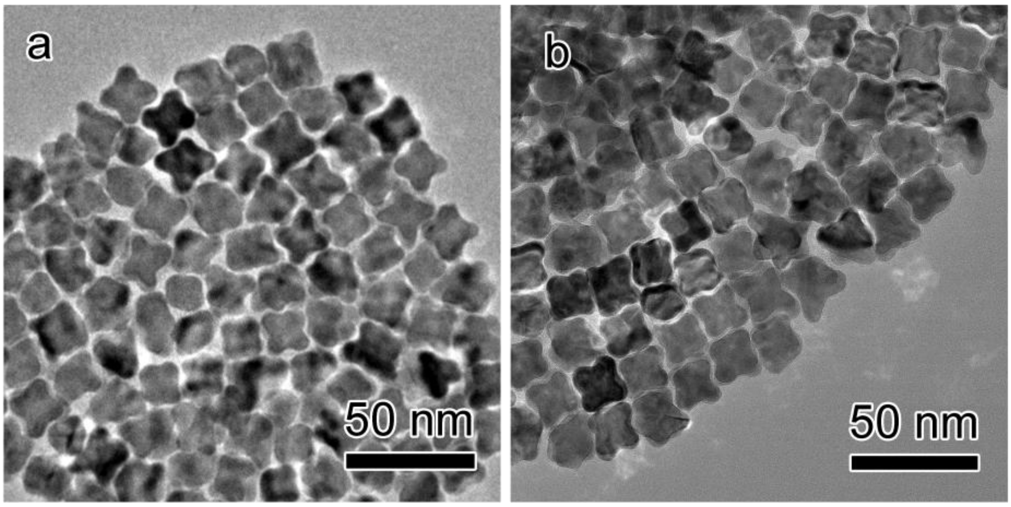

Figure S4. TEM images of PtCu nanocrystals obtained with the following conditions: (a) 23 mg of TBAB + 50 mg of TOPO and (b) 9 mg of KBr + 50 mg of TOPO.

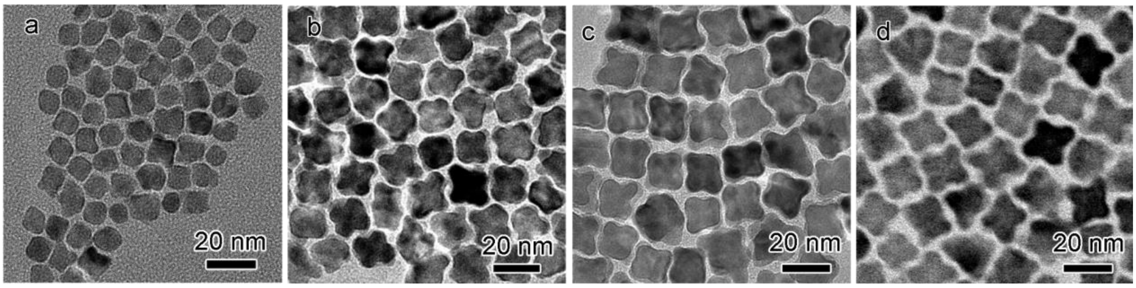

Figure S5. TEM images of intermediates obtained at different reaction periods. (a) 240 ^{o}C, (b) 260 ^{o}C 5 min, (c) 260 ^{o}C 30 min, and (d) 260 ^{o}C 1 h.

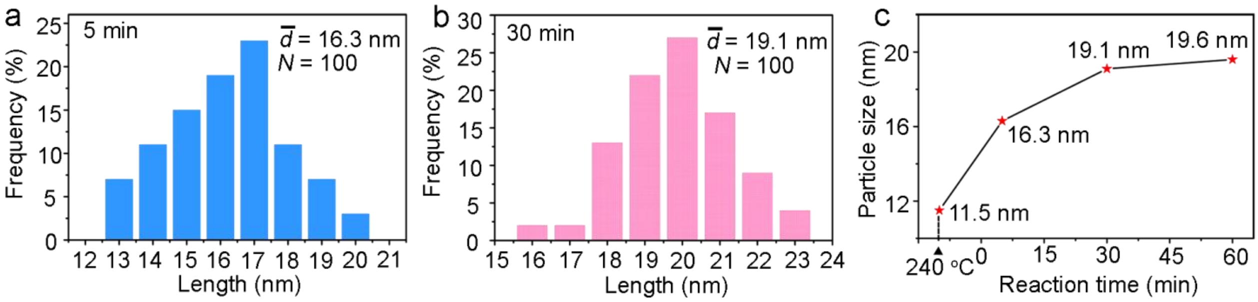

Figure S6. Particle size distributions of intermediates at different reaction periods. (a) 240 ^{o}C, (b) 260 ^{o}C 5 min, and (c) changes of particle sizes.

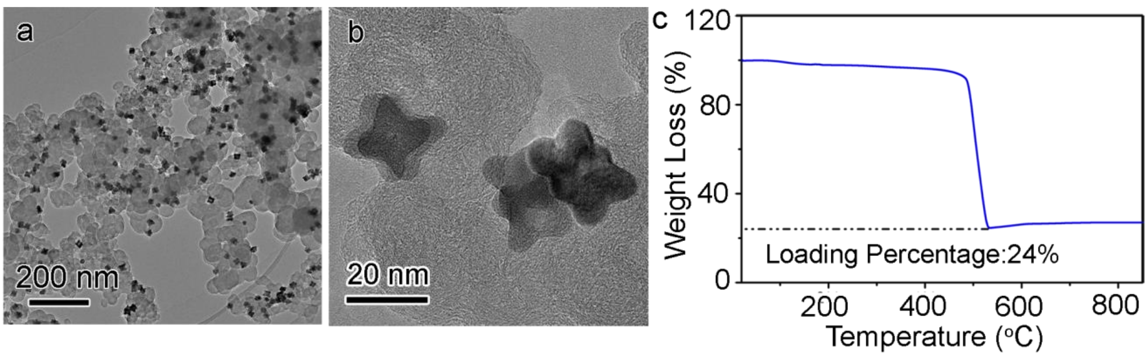

Figure S7. (a) TEM image, (b) HRTEM image, and (c) TGA curve of the $PtCu_3/C$ catalyst.

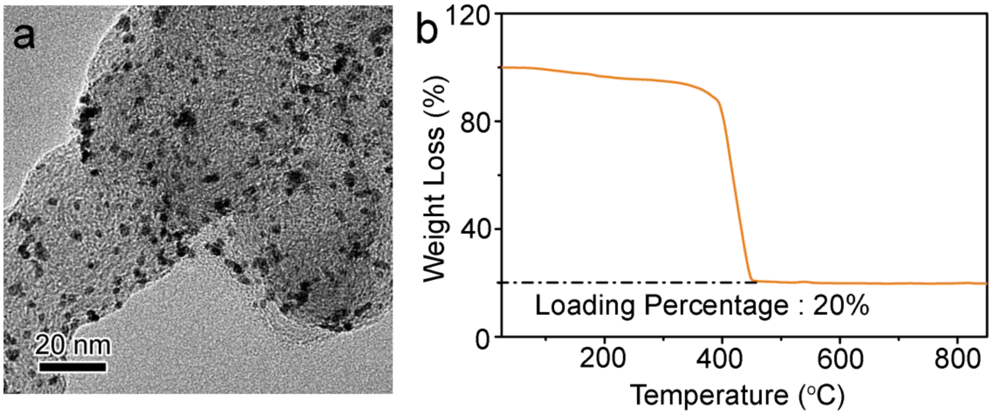

Figure S8. (a) TEM image and (b) TGA curve of the commercial Pt/C.

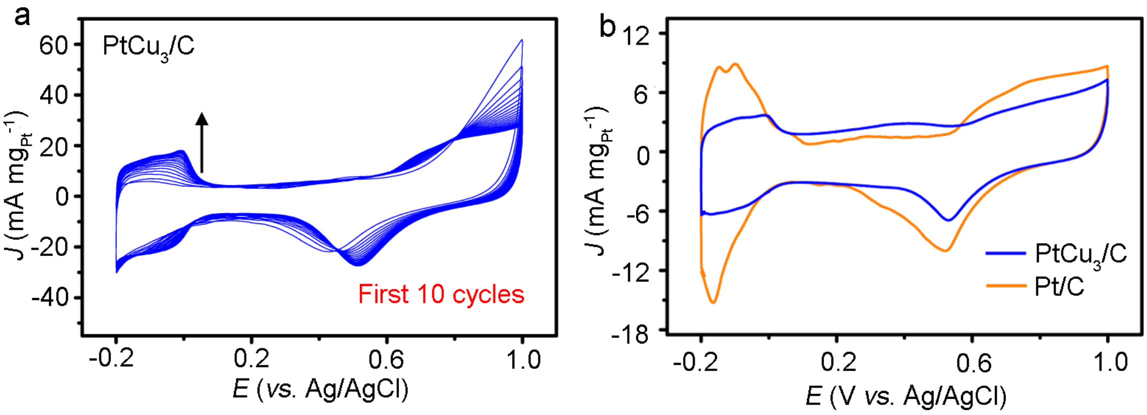

Figure S9. (a) CV curves of the $PtCu_3$ concave nanocubes recorded in Ar-saturated 0.5 M H_2SO_4 at 50 mV s^{-1} for first 10 cycles and (b) CV curves of the $PtCu_3$ concave nanocubes and commercial Pt/C recorded in Ar-saturated 0.5 M H_2SO_4 at 10 mV s^{-1}.

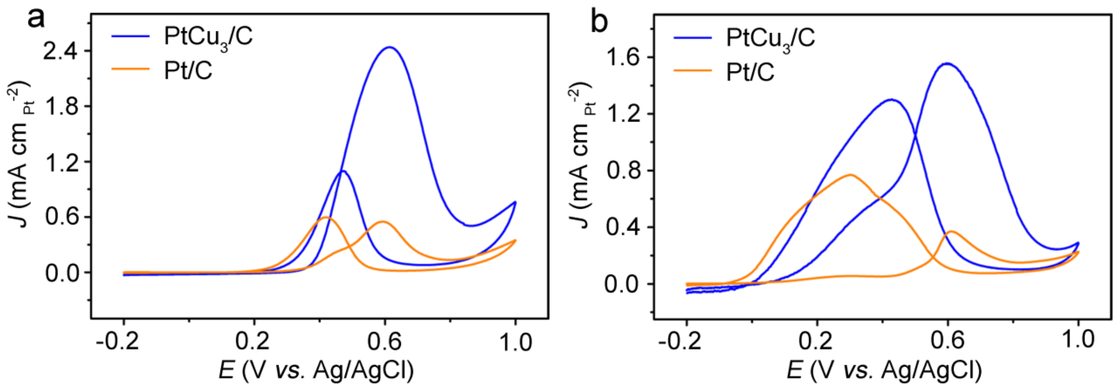

Figure S10. (a) CV curves (normalized by $ECSA_H$) recorded in Ar-saturated 0.5 M H_2SO_4 + 1.0 M CH_3OH solution at 10 mV s^{-1} and (b) CV curves (normalized by $ECSA_H$) recorded in Ar-saturated 0.50 M H_2SO_4 + 0.25 M HCOOH solution at 10 mV s^{-1}.

Table S2. Electrocatalytic performance of Pt-based nanocrystals.

Materials	Methanol Oxidation			Formic Acid Oxidation			Ref
	J_m	J_s	Electrolyte	J_m	J_s	Electrolyte	
$PtCu_3$ concave nanocubes	0.69	2.44	0.5 M H_2SO_4 1.0 M CH_3OH 10 mV s^{-1}	0.45	1.57	0.50 M H_2SO_4 0.25 M HCOOH 10 mV s^{-1}	This Work
Excavated rhombic dodecahedral $PtCu_3$ alloy	-	-	-	0.815	3.15	0.5 M H_2SO_4 0.25 M HCOOH 50 mV s^{-1}	7
Mesoporous PtCu alloy nanoparticles	0.314	1.39	0.5 M H_2SO_4 1.0 M CH_3OH 50 mV s^{-1}	-	-	-	8
Pt-Cu hierarchical trigonal bipyramid nanoframes	-	-	-	0.64	3.77	0.5 M H_2SO_4 0.25 M HCOOH 50 mV s^{-1}	9
Cu_5Pt Dodecahedra nanoframes	-	-	-	0.194	10.89	0.5 M H_2SO_4 1.0 M HCOOH 50 mV s^{-1}	10
Pt_3Cu icosahedra	0.736	2.14	0.1 M $HClO_4$ 0.2 M CH_3OH 50 mV s^{-1}	-	-	-	11
PtRu nanowires	0.82	1.16	0.1 M $HClO_4$ 0.5 M CH_3OH 50 mV s^{-1}	-	-	-	12
Pt-Ni concave nanocubes	-	1.86	0.5 M H_2SO_4 2 M CH_3OH 50 mV s^{-1}	-	0.45	0.5 M H_2SO_4 1.0 M CH_3OH 50 mV s^{-1}	13
Excavated cubic Pt-Sn nanocrystals	-	2.30	0.5 M H_2SO_4 0.5 M CH_3OH 50 mV s^{-1}	-	-	-	14

J_m (A mg_{Pt}^{-1}): mass activity J_s (mA cm_{Pt}^{-2}): specific activity

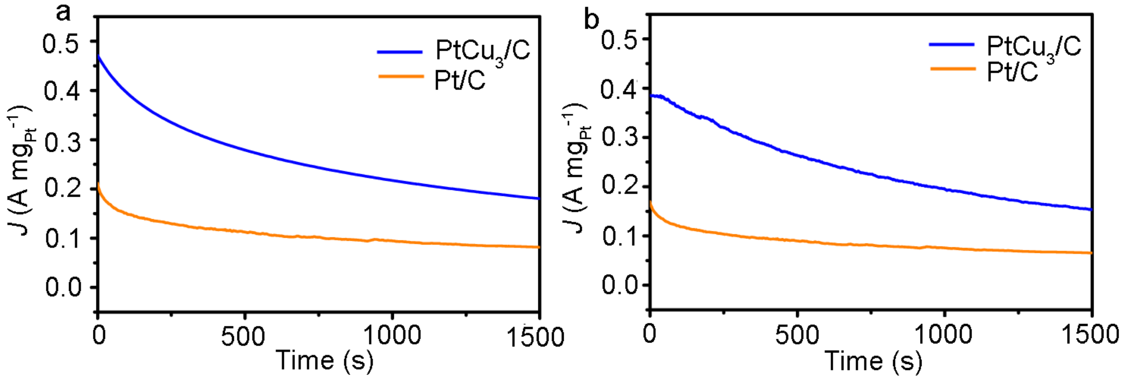

Figure S11. Chronoamperometric curves of (a) methanol oxidation recorded at 0.5 V and (b) formic acid oxidation recorded at 0.5 V.

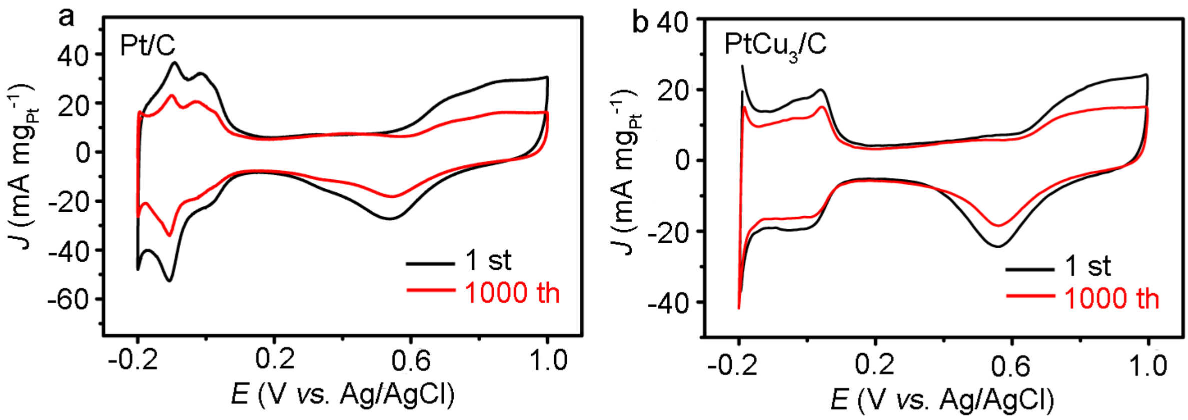

Figure S12. CV curves of (a) the commercial Pt/C and (b) $PtCu_3/C$ recorded in Ar-saturated 0.5 M H_2SO_4 at 50 mV s^{-1} before and after durability tests.

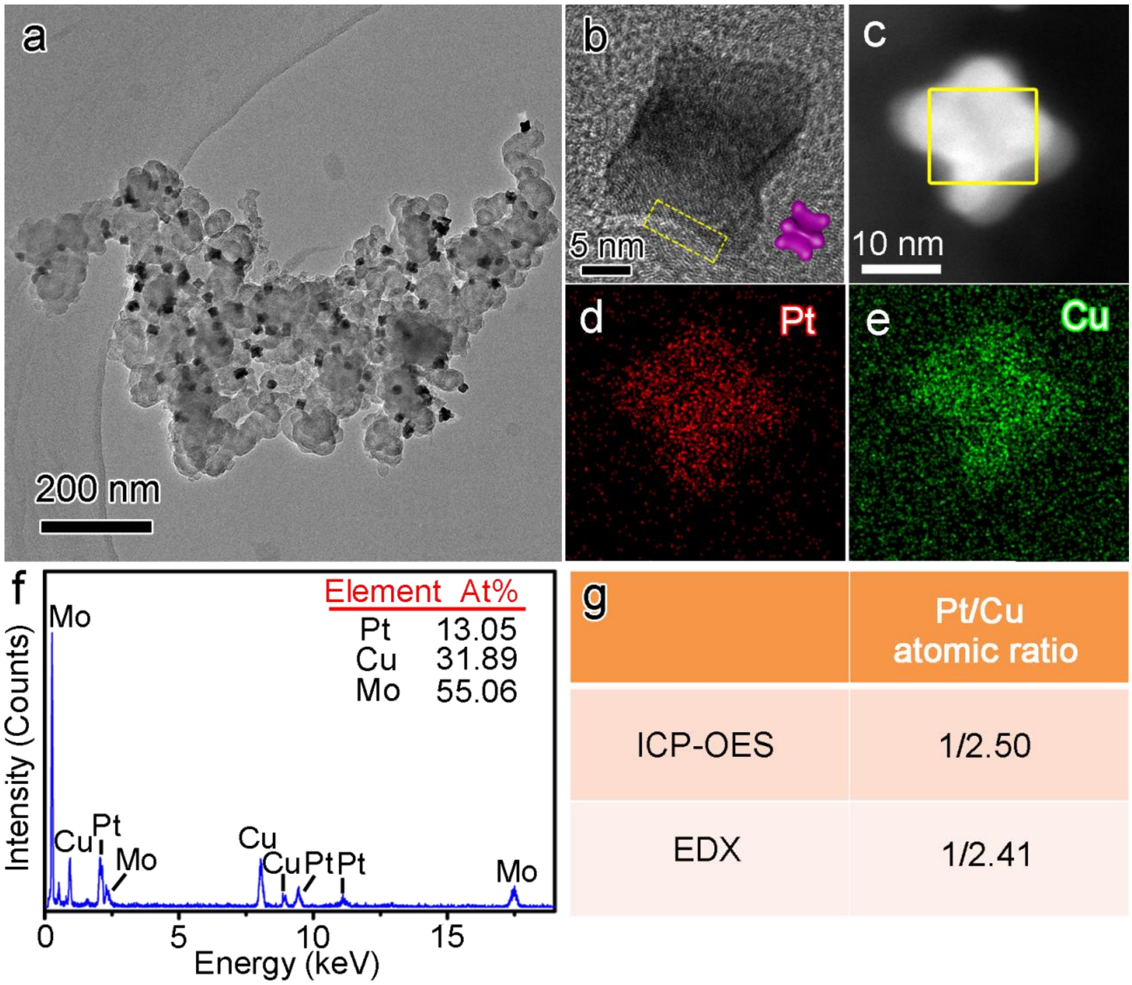

Figure S13. (a) TEM image of the $PtCu_3$/C, (b) HRTEM image and the structural model, (c) HAADF-STEM images (d, e) EDS mappings, (f) EDS spectra as indicated by a yellow rectangle in (c), and (g) atomic ratios of the $PtCu_3$ concave nanocubes after accelerated durability test. (Mo is from the TEM grids.)

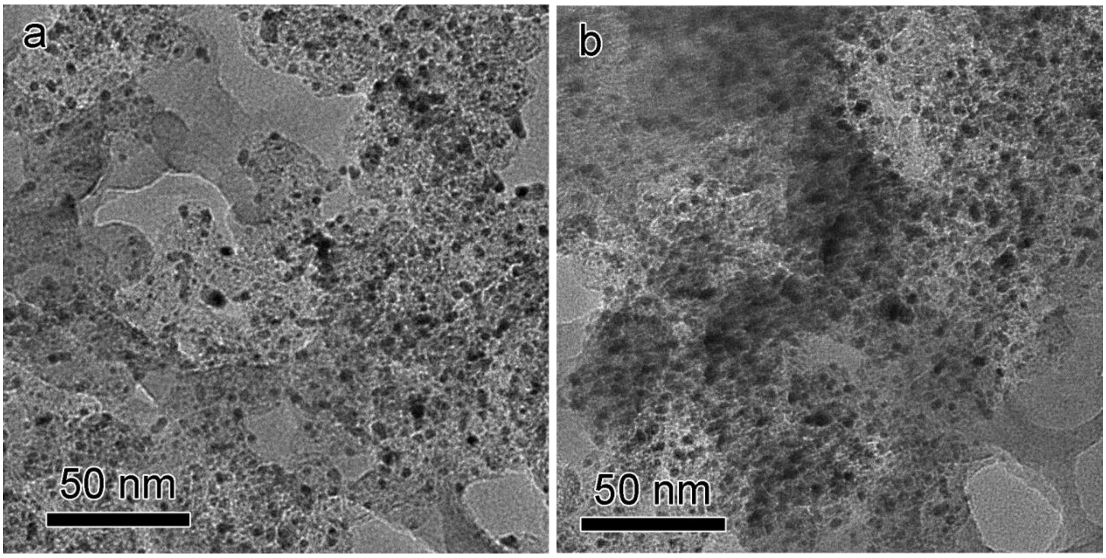

Figure S14. TEM images of the commercial Pt/C after accelerated durability test.

Table S3. Ratios of I_f / I_b for methanol and formic acid oxidation, $ESCA_H$: $ECSA_{CO}$, and peak potentials of CO oxidation for the $PtCu_3$/C catalyst and commercial Pt/C.

	methanol oxidation I_f / I_b	formic acid oxidation I_f / I_b	$ESCA_H$: $ECSA_{CO}$	peak potential of CO oxidation
$PtCu_3$/C	2.27	0.90	1.04 : 1.00	0.45 V
Pt/C	0.93	0.45	1.00 : 1.11	0.54 V

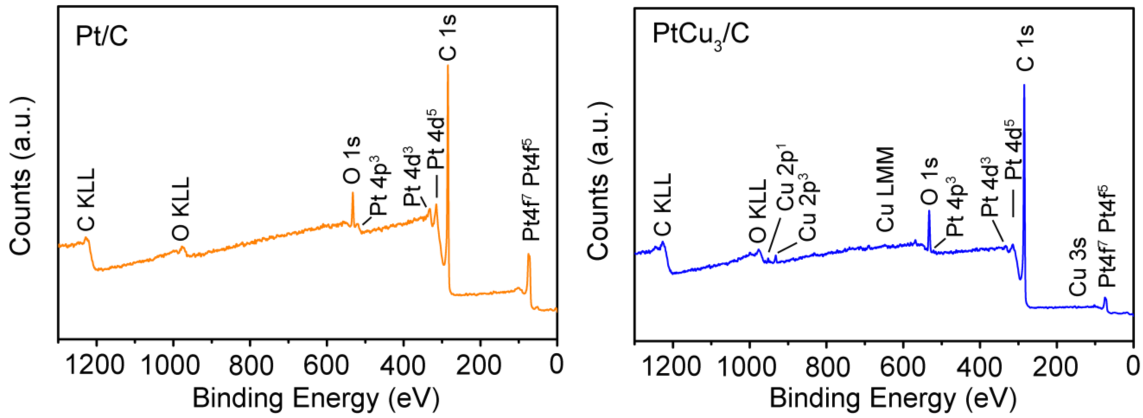

Figure S15. XPS spectra of the Pt/C and $PtCu_3$/C.

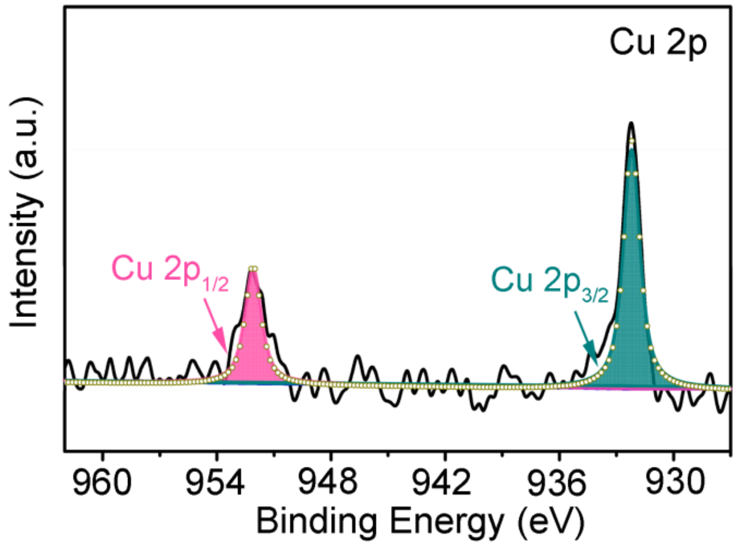

Figure S16. XPS spectrum of the as-prepared $PtCu_3/C$ catalyst in Cu 2p region.

References

(1) Becknell, N.; Son, Y.; Kim, D.; Li, D.; Yu, Y.; Niu, Z.; Lei, T; Sneed, B. T.; More, K. L.; Markovic, N. M.; Stamenkovic, V. R.; Yang, P. Control of Architecture in Rhombic Dodecahedral Pt-Ni Nanoframe Electrocatalysts. *J. Am. Chem. Soc.* **2017**, *139*, 11678−11681.

(2) Shi, J.; Lei, K.; Sun, W.; Li, F.; Cheng, F.; Chen, J. Synthesis of size-controlled $CoMn_2O_4$ quantum dots supported on carbon nanotubes for electrocatalytic oxygen reduction/evolution. *Nano Research* **2017**, *10*, 3836−3847.

(3) Jia, Y.; Jiang, Y.; Zhang, J.; Zhang ,L.; Chen, Q.; Xie, Z.; Zheng, L. Unique Excavated Rhombic Dodecahedral $PtCu_3$ Alloy Nanocrystals Constructed with Ultrathin Nanosheets of High-Energy {110} Facets. *J. Am. Chem. Soc.* **2014**, *136*, 3748−3751.

(4) Puzder, A.; Williamson, A. J.; Zaitseva, N.; Galli, G. The effect of organic ligand binding on the growth of CdSe nanoparticles probed by ab initio calculations. *Nano Lett*, **2004**, *4*, 2361−2365.

(5) Ma, Y.; Yin, L.; Yang, T.; Huang, Q.; He, M.; Zhao, H.; Zhang, D.; Wang, M.; Tong, Z. One-Pot Synthesis of Concave Platinum-Cobalt Nanocrystals and Their Superior Catalytic Performances for Methanol Electrochemical Oxidation and Oxygen Electrochemical Reduction. *ACS Appl. Mater Interfaces* **2017**, *9*, 36164−36172.

(6) Zhu, Z.; Shi, X.; Zhu, D.; Wang, L.; Lei, K.; Li, F. A Hybrid Na//K^+-Containing Electrolyte//O_2 Battery with High Rechargeability and Cycle Stability. *Research* **2019**, *2019*, 6180615.

(7) Jia, Y.; Jiang, Y.; Zhang, J.; Zhang, L.; Chen, Q.; Xie, Z, Zheng, L. Unique Excavated Rhombic Dodecahedral $PtCu_3$ Alloy Nanocrystals Constructed with Ultrathin Nanosheets of High-Energy {110} Facets. *J. Am. Chem. Soc.* **2014**, *136*, 3748−3751.

(8) Kang, Y.; Jiang, B.; Alothman, Z. A.; Badjah, A. Y.; Naushad, Mu.; Habila, M.; Wabaidur, Saikh.; Henzie, Joel.; Li, H.; Yamauchi, Y. Mesoporous PtCu Alloy

Nanoparticles with Tunable Compositions and Particles Sizes Using Diblock Copolymer Micelle Templates. *Chem. Eur.- J.* **2018**, *24*, 1−7.

(9) Chen, S.; Su, H.; Wang, Y.; Wu, W.; Zeng, J. Size-Controlled Synthesis of Platinum-Copper Hierarchical Trigonal Bipyramid Nanoframes. *Angew. Chem., Int. Ed*. **2015**, *54*, 108−113.

(10) Wang, Y.; Jiang, Xian.; Fu, G.; Li, Y.; Tang, Y.; Lee, J.; Tang, Y. Cu_5Pt Dodecahedra with Low-Pt Content: Facile Synthesis and Outstanding Formic Acid Electrooxidation. *ACS Appl. Mater. Interfaces* **2019**, *11*, 34869−34877.

(11) Sun, X.; Jiang, K.; Zhang, N.; Guo. S.; Huang, X. Crystalline Control of {111} Bounded Pt_3Cu Nanocrystals: Multiply-Twinned Pt_3Cu Icosahedra with Enhanced Electrocatalytic Properties. *ACS Nano* **2015**, *9*, 7634−7640.

(12) Huang, L.; Zhang, X.; Wang. Q.; Han, Y.; Fang, Y.; Dong, S. Shape-Control of Pt-Ru Nanocrystals: Tuning Surface Structure for Enhanced Electrocatalytic Methanol Oxidation. *J. Am. Chem. Soc.* **2018**, 140, *3*, 1142−1147.

(13) Xu, X.; Zhang, X.; Sun, H.; Yang, Y.; Dai, X.; Gao, J.; Li, X.; Zhang, P.; Wang, H.; Yu, N.; Sun, S. Synthesis of Pt-Ni Alloy Nanocrystals with High-Index Facets and Enhanced Electrocatalytic Properties. *Angew. Chem., Int. Ed*. **2014**, *126*, 12730−12735.

(14) Chen, Q, Yang, Y.; Cao, Z.; Kuang, Qin.; Du, G.; Jiang, Y.; Xie, Z.; Zheng, L. Excavated Cubic Platinum–Tin Alloy Nanocrystals Constructed from Ultrathin Nanosheets with Enhanced Electrocatalytic Activity. *Angew. Chem., Int. Ed.* **2016**, *55*, 9021−9025.